Science of the Total Environment 917 (2024) 170457

Contents lists available at ScienceDirect

Science of the Total Environment

journal homepage: www.elsevier.com/locate/scitotenv

Exceptionally low mercury concentrations and fluxes from the 2021 and 2022 eruptions of Fagradalsfjall volcano, Iceland

Brock A. Edwards [a,b], Melissa A. Pfeffer [c], Evgenia Ilyinskaya [d], Barbara I. Kleine-Marshall [e], Céline L. Mandon [f], Adam Cotterill [g], Alessandro Aiuppa [h], Peter M. Outridge [a,b], Feiyue Wang [a,*]

[a] Centre for Earth Observation Science and Department of Environment and Geography, University of Manitoba, Winnipeg, Manitoba R3T 2N2, Canada
[b] Geological Survey of Canada, Natural Resources Canada, Ottawa, Ontario K1A 0E8, Canada
[c] Icelandic Meteorological Office, 105 Reykjavík, Iceland
[d] COMET, School of Earth and Environment, University of Leeds, Leeds LS2 9JT, United Kingdom
[e] GeoZentrum Nordbayern, Friedrich-Alexander-Universitaet Erlangen-Nuremberg, 91054 Erlangen, Germany
[f] Institute of Earth Sciences, University of Iceland, 101 Reykjavík, Iceland
[g] Department of Earth Sciences, University College London, London WC1E 6BS, United Kingdom
[h] Università di Palermo, Dipartimento di Scienze della Terra e del Mare (DiSTeM), 90123 Palermo, Italy

HIGHLIGHTS

- Lowest mercury concentrations and fluxes reported for any active volcano on Earth
- Iceland volcanic systems appear to be sourced from a particularly Hg-poor mantle.
- Simultaneous near-vent and downwind data suggest Hg/SO_2 is conserved over distance.
- First drone-based measurements of plume gaseous mercury above an erupting volcano
- Drone-based volcanic mercury sampling now feasible and should be the preferred method.

GRAPHICAL ABSTRACT

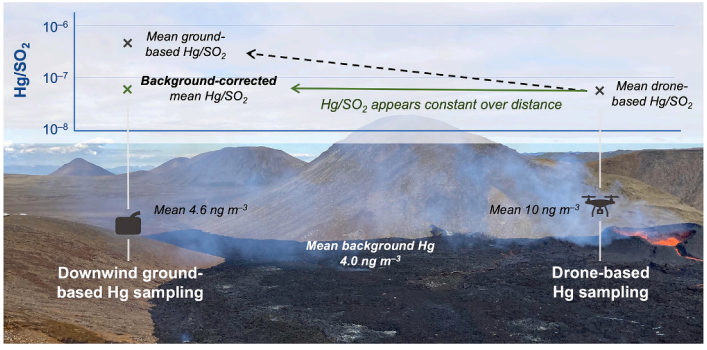

ARTICLE INFO

Editor: Xinbin Feng

Keywords:
Volcanic emissions
Sulfur dioxide
Hg/SO_2
Drones
Natural emissions

ABSTRACT

Mercury (Hg) is naturally released by volcanoes and geothermal systems, but the global flux from these natural sources is highly uncertain due to a lack of direct measurements and uncertainties with upscaling Hg/SO_2 mass ratios to estimate Hg fluxes. The 2021 and 2022 eruptions of Fagradalsfjall volcano, southwest Iceland, provided an opportunity to measure Hg concentrations and fluxes from a hotspot/rift system using modern analytical techniques. We measured gaseous Hg and SO_2 concentrations in the volcanic plume by near-source drone-based sampling and simultaneous downwind ground-based sampling. Mean Hg/SO_2 was an order of magnitude higher at the downwind locations relative to near-source data. This was attributed to the elevated local background Hg at ground level (4.0 ng m^{-3}) likely due to emissions from outgassing lava fields. The background-corrected plume Hg/SO_2 mass ratio (5.6×10^{-8}) therefore appeared conservative from the near-source to several hundred meters distant, which has important implications for the upscaling of volcanic Hg fluxes based on SO_2 measurements.

* Corresponding author.
E-mail address: feiyue.wang@umanitoba.ca (F. Wang).

https://doi.org/10.1016/j.scitotenv.2024.170457
Received 19 September 2023; Received in revised form 22 January 2024; Accepted 24 January 2024
Available online 1 February 2024

Using this ratio and the total SO_2 flux from both eruptions, we estimate the total mass of gaseous Hg released from the 2021 and 2022 Fagradalsfjall eruptions was 46 ± 33 kg, equivalent to a flux of 0.23 ± 0.17 kg d^{-1}. This is the lowest Hg flux estimate in the literature for active open-conduit volcanoes, which range from 0.6 to 12 kg d^{-1} for other hotspot/rift volcanoes, and 0.5–110 kg d^{-1} for arc volcanoes. Our results suggest that Icelandic volcanic systems are fed from an especially Hg-poor mantle. Furthermore, we demonstrate that the aerial near-source plume Hg measurement is feasible with a drone-based active sampling configuration that captures all gaseous and particulate Hg species, and recommend this as the preferred method for quantifying volcanic Hg emissions going forward.

1. Introduction

Volcanoes emit mercury (Hg) to the atmosphere. The main Hg form released from such geogenic sources is gaseous elemental mercury (GEM) (Martin et al., 2011), which has a long atmospheric lifetime of ~6 months (Horowitz et al., 2017), facilitating its global transport and dispersal (Bagnato et al., 2014; Lindberg et al., 2007). Mercury can therefore be carried potentially thousands of km away from the original source before being deposited onto surface environments, typically as gaseous oxidized mercury (GOM) or particulate-bound mercury (PBM) (Schroeder and Munthe, 1998). Upon conversion to methylmercury compounds, primarily via microbial activity in the aquatic environment, Hg accumulates in living organisms and can lead to toxic exposure for humans and other life forms (AMAP/UNEP, 2019).

Annual global atmospheric Hg fluxes have been estimated for anthropogenic emissions (2500 t a^{-1}) and ocean evasion (3400 t a^{-1}; AMAP/UNEP, 2019). However, fluxes from natural sources such as volcanic degassing are highly uncertain, with implications for global Hg emissions modelling and regulation (Edwards et al., 2021; Wang et al., 2019), as well as for Hg exposure risk assessments in regions around volcanoes (Calabrese et al., 2011; Ferrara et al., 2000).

As detailed in Edwards et al. (2021), a major source of uncertainty in the global volcanic Hg flux estimate is the use of Hg-to-sulfur dioxide (SO_2) mass ratios to upscale Hg fluxes on individual (i.e., volcano-specific) and regional scales. With this method, Hg/SO_2 is calculated from simultaneous measurements of these two gases at a fixed point in the volcanic plume. Often these are short-term "spot measurements" made at locations with some distance from the crater or vent, as dictated by topography, accessibility and safety, as well as the prevailing direction of the winds that transport the volcanic plume toward the sampling location (Edwards et al., 2021). From these spot measurements, the Hg flux is then estimated based on SO_2 flux measurements from ground- and/or satellite-based instruments, under the assumption that the Hg/SO_2 mass ratio does not vary considerably in the plume (Bagnato et al., 2014; Fischer and Chiodini, 2015).

The large range of literature Hg/SO_2 values, coupled with the difficulty in adequately sampling the continuously changing volcanic plume, mean that scaled-up global volcanic Hg flux estimates vary widely (0.6–1000 t a^{-1}; Ferrara et al., 2000; Nriagu, 1989; Pyle and Mather, 2003; Varekamp and Buseck, 1981, 1986). With recent improvements in atmospheric Hg analytical methods and in emission budgets for other sources, some of the earlier estimates have been ruled out as erroneous or at least highly unlikely (Bagnato et al., 2014; Edwards et al., 2021; Pyle and Mather, 2003). Consequently, this range has recently been narrowed to 37–250 t a^{-1} (Bagnato et al., 2011, 2014; Li et al., 2020; Sonke et al., 2023; Zhang et al., 2023).

Nevertheless, this field of research continues to be hindered by a lack of information about inter-volcano variability of Hg fluxes, long- and short-term temporal changes in Hg emissions, and ultimately the suitability of extrapolating a handful of volcanic Hg fluxes to a global emissions figure (Edwards et al., 2021). It follows that constraining the global volcanic Hg flux will likely not be accomplished by further scrutinizing the sparse available data, but rather by continued field measurements at degassing volcanoes—by adding incrementally to a global dataset incorporating the continuous "passive degassing" of different types of active volcanoes, as well as the rarer short-term explosive and effusive eruptions. To this end, here we present new Hg emissions data from the 2021 and 2022 fissure eruptions of Fagradalsfjall volcano, Iceland. These two eruptions were characterized by variable but long-lived gas and aerosol emissions, effusive lava outflows and almost no explosivity. Our gas sampling approach included aerial drone-based collections of the volcanic plume directly above the actively erupting vent, a first for volcanic Hg research.

2. Materials and methods

2.1. Field site

The Reykjanes Peninsula in southwest Iceland is the on-land continuation of the Mid-Atlantic Reykjanes spreading ridge (Thordarson and Höskuldsson, 2022; Fig. 1). It is built from the lava flows of six major southwest–northeast striking volcanic systems characterized by strike–slip and normal faulting, episodic rifting, and basaltic fissure eruptions (Arnórsson, 1995; Sæmundsson et al., 2020). Between the Krýsuvík-Trölladyngja and Svartsengi systems lies the primitive Fagradalsfjall volcanic system, which was last active over 6000 years ago and lacks any associated surface geothermal activity (Sigurgeirsson and Sæmundsson, 2022).

After more than a year of volcano-tectonic unrest, a magmatic dike intrusion reached the surface and a small basaltic fissure eruption began on 19 March 2021 in Geldingadalir valley (63°53′20.0"N, 22°16′13.4"W), between the tuyas and massifs of the Fagradalsfjall table mountain complex (Halldórsson et al., 2022). Within a few weeks, several vents opened along the northeast–southwest oriented dike line, and lava pooled in Geldingadalir and spilled over into the neighbouring Meradalir valley (Barsotti et al., 2023). At the end of April, the eruption entered a new phase, with fountaining activity and increased lava discharge from a single vent. The 2021 eruption officially ended on September 18, after half a year (182 days).

On 3 Aug 2022, another eruption began at Fagradalsfjall ~0.5 km northeast of Geldingadalir on the northern edge of Meradalir (63°53′56.4"N, 22°14′56.4"W). The fissure eruption produced basaltic lava flows with a slightly more geochemically evolved composition than the 2021 lavas, but sourced from the same dominantly peridotitic mantle source at 15–20 km depth (Halldórsson et al., 2022; Krmíček et al., 2022). After two and a half weeks of activity, lava effusion and magmatic gas emissions ceased on August 21. The two eruptions combined lasted for 200 days.

2.2. Ground-based gas sampling

Field sampling campaigns were conducted 31 Mar–14 Apr 2021 (Geldingadalir eruption) and 12–21 Aug 2022 (Meradalir eruption). We measured GEM, SO_2 and other major gases in volcanic plumes downwind of the main vent on five separate days. Sampling locations (see Fig. 1) at both sites shifted from day to day due to changes in lava field coverage, vent system activity and wind direction, and varied in duration from 35 to 110 min.

2.2.1. GEM measurements

Atmospheric GEM concentrations were measured in real time using a portable atomic absorption spectrometer (Lumex RA-915 M mercury analyzer; Lumex Instruments, St. Petersburg, Russia). The Lumex pumps air through the instrument's multi-path detection cell at a flow rate of 10 L min^{-1}, with GEM concentration data acquired every 10 s (detection limit: 0.5 ng m^{-3}). An automatic 1-min zero correction is initiated every 15 min to correct for baseline drift during sampling, and the instrument's precision was tested using the self-test function before and after each sampling run. Relative standard deviation (*D*) values within ±20 % are required for reliable data; for this work, *D* values were always within ±5 %. The Lumex was calibrated by the manufacturer before and after each fieldwork campaign; the calibrations did not change significantly during either campaign (see Edwards et al., 2023).

2.2.2. MultiGAS SO_2 measurements

Plume SO_2 concentrations were detected in real time using a multi-component gas analyzer system (MultiGAS) which measures SO_2, H_2S, CO_2 and H_2 at 1 s intervals (described in Aiuppa et al., 2005, 2010). The MultiGAS draws in air at 1.2 L min^{-1} through a 1-μm particle filter and a series of integrated sensors consisting of an infrared spectrometer for CO_2 (Edinburgh Instruments, range 0–3000 ppmv), electrochemical sensors for SO_2 (CiTiceL series T3ST/F, range 0–200 ppmv), H_2S (CiTiceL series T3H, range 0–200 ppmv), and H_2 (CiTiceL series T3HYT, range 0–200 ppmv), and a relative humidity/temperature sensor (Galltec-Mela thermo-hygrometer; range 0–100 % relative humidity). Instrumental calibration with standard reference gases at the Università di Palermo, Italy, was performed before and after the field campaigns. For the purposes of complementing other ground-based SO_2 observations (see Section 2.4) and estimating Hg/SO_2 ratios, this study will mainly discuss SO_2 concentration measurements. Data for other major gases are summarized in Table S1. For ground-based measurements, we estimate an instrumental uncertainty of ~10 % based on the relative uncertainties of the Lumex (± 5 %) and MultiGAS sensors (± 2 %; Aiuppa et al., 2010).

2.3. Aerial (drone-based) gas sampling

2.3.1. PBM and TGM measurements

On 6 April 2021, a filter pack sampler mounted on a quadcopter drone (model Matrice 300; DJI, Shenzhen, China) was used to collect PBM near the Geldingadalir eruption site in conjunction with a suite of other trace metals and acid gases. The filter pack assembly contained a Whatman PTFE 47-mm diameter 1.0-μm pore size filter (used to collect PBM) followed by 3 alkali-impregnated gas filters (see Ilyinskaya et al., 2017, 2021). Air flow was generated using an SKC Leland Legacy pump at a rate of 14 L min^{-1}. The drone-mounted sampler was flown on three flights in the relatively dense plume at ~75 m height starting from approximately 2 km from the eruption site, for a cumulative flight time of 45 min and pumped air volume of 640 L. Immediately after sampling, the filter pack was sealed with Parafilm and double-bagged to prevent contamination during transport.

Near-source aerial Hg measurements of the plume were made by mounting an activated carbon trap (ACT) sampler on the same drone described above (Fig. 2). The ACT sampler collects total gaseous mercury (TGM = GEM + GOM), including reactive oxidized Hg species (e.g., $HgCl_2$, $HgBr_2$, HgO; US EPA, 2016a), and consists of a 10-mm diameter iodide-impregnated activated carbon sorbent trap in a glass housing (Apex Instruments, Fuquay-Varina, USA, part number MTB-U) attached to a battery-powered portable pump (Buck Elite-5; A.P. Buck Inc., Orlando, USA) with a set flow rate of 3 L min^{-1} (Edwards et al., 2023). An in-line flowmeter was used before and after ACT sampling runs to check flow rate accuracy. The activated carbon sorbent trap is separated into primary and secondary segments in series, with the secondary meant to catch any TGM break-through from the primary segment due to trap saturation or other collection issues (US EPA, 2016a). Glass wool

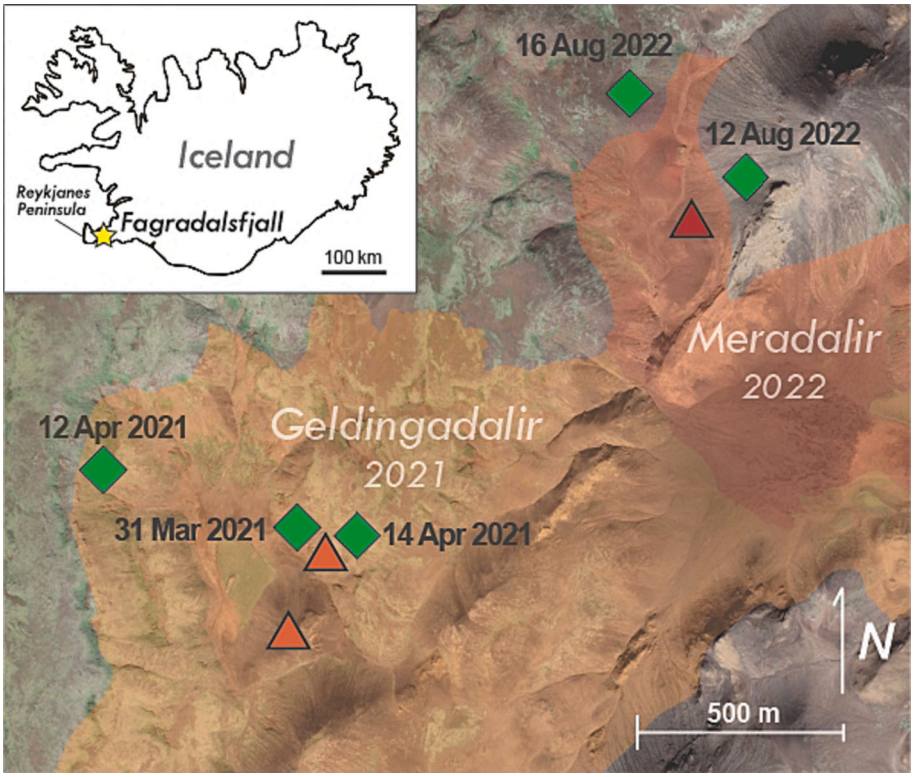

Fig. 1. Satellite map of study site with overlay of Geldingadalir and Meradalir lava flows, the main active vents during the field campaigns of 2021 (orange triangles) and 2022 (red triangle), and ground-based sampling locations (green diamonds) with annotated dates.
(Map created with ArcGIS and Google Earth Pro; lava field overlays are based on maps by Benjamin Hennig (GeoVis Lab, University of Iceland, geovis.hi.is).)

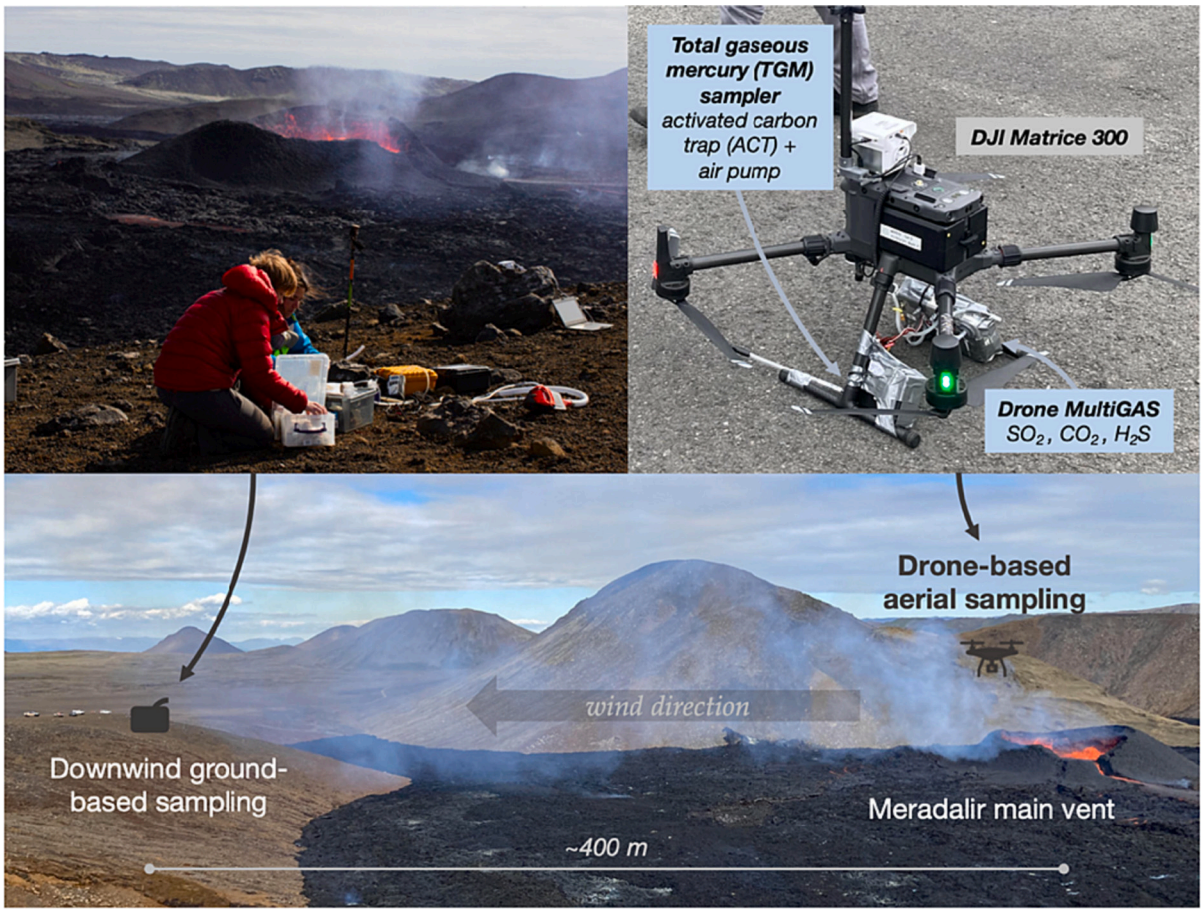

Fig. 2. Image of the Meradalir main vent on 16 Aug 2022, with approximate sampling locations and drone-based sampling configuration. Top left photo by Eemu Ranta.

filter plugs are positioned upstream of each segment to filter out particulate matter ≥8 μm in diameter.

On two sampling days (12 and 16 Aug 2022) the drone was flown from a nearby (~400 m distant) launch site to the active Meradalir vent where it hovered at 75–100 m above ground level in the concentrated near-vent plume, collecting TGM on the ACT while simultaneously measuring major gases using a MultiGAS (see Section 2.3.2; Fig. 2). On 21 Aug 2022, drone flights were made several hours after the cessation of magmatic emissions and eruptive activity, and the instruments sampled air above several steaming areas near the main vent. Each drone field day consisted of multiple flights (3–5 per day) with in-plume sampling times ranging from 15 to 25 min. Regular "pit stop" landings back at the launch site facilitating the replacement of drone batteries, during which the instruments were paused and the sampling inlets sealed. The ACT sampler was therefore measuring out-of-plume background air as the drone travelled to and from the launch site, but the transit time was short relative to the cumulative in-plume sampling time (1–2 min in total per flight, or < 10 % total sampling time) and is not expected to significantly affect the results.

It should be noted that due to aircraft payload limitations, there were no replicate ACT or filter pack samples collected for any of the drone flights; the sample number per flight day is therefore one, representing Hg collected on multiple consecutive flights with large cumulative sampling times. This approach is preferred over collecting several samples of shorter duration, as the amount of sampled material is sufficient to be significantly above detection limits for trace elements such as Hg.

2.3.2. Drone MultiGAS SO_2 measurements

A miniaturized version of the MultiGAS described above (Drone MultiGAS, Università di Palermo) was mounted on the same UAS used for filter pack sampling (see Section 2.2.2) for aerial SO_2. The Drone MultiGAS pumps air at 1.0 L min^{-1} through a 1-μm particle filter across an infrared spectrometer for CO_2 (SmartGAS FlowEvo; range 0–1000 ppmv, ± 1 % noise and ± 1 ppm precision) and sensors for SO_2 (CiTiceL series T3ST/F, range 0–200 ppmv) and H_2S (CiTiceL series T3H, range 0–50 ppmv), acquiring concentration data at 1 s intervals. Instrumental calibration with standard reference gases at the Università di Palermo was performed before and after fieldwork.

The relative uncertainty associated with the ACT pump flow rate is estimated as 15–20 % based on fluctuations in flowmeter readings noted in the field. Combining this with the MultiGAS analytical sensor uncertainties referenced above, we estimate a total uncertainty of ~20 %.

2.4. Offline sample analyses

All sorbent trap material and particulate filters were shipped to the University of Manitoba and analyzed for total Hg by atomic absorption spectroscopy on a Hydra IIc Total Mercury Analyzer (Teledyne Leeman Labs, Mason, OH, USA) following the standard method outlined in US EPA Method 7473 (US EPA, 1998) and described previously (Edwards et al., 2023). Total Hg was quantified based on calibration curves obtained with the National Research Council of Canada certified reference materials (CRM) MESS-4 (mean concentration 90 ± 40 ng g^{-1} Hg) and PACS-3 (mean concentration 2980 ± 360 ng g^{-1} Hg). To verify instrumental accuracy, MESS-4 and another CRM, NIST 2709a (mean concentration 900 ± 200 ng g^{-1} Hg; National Institute of Standards and

Technology, Gaithersburg, USA) were analyzed every 10–15 samples. Results of CRMs were deemed valid when concentrations fell within the standard deviation reported by the manufacturer. Whenever these were outside the acceptable range, two additional CRMs were analyzed; if these were also out of range, a new calibration curve was constructed. Mean CRM recoveries were 103 ± 8.5 %.

The method detection limit (MDL) was calculated following US EPA (2016b). Briefly, after field blank concentrations for carbon sorbent and particulate filters were determined ($n = 5$), their standard deviation was multiplied by the t statistic for the corresponding degrees of freedom from the single-tailed 99th percentile t table (3.747; US EPA, 2016b). The resulting MDL for Hg concentration determinations was 0.02 ng; all results below this are reported as < MDL.

2.5. Data processing and statistical analyses

For the purposes of analyzing simultaneous plume concentrations of GEM and SO_2, MultiGAS data (collected at 1 s intervals) were averaged over 10 s intervals to match the Lumex data, in both timing and resolution. The same was done for drone SO_2 data but not for drone TGM, because this is a single time-averaged concentration calculated from ACT sampling. The combined GEM/SO_2 concentration data were then filtered for in-plume intervals to ensure data were representative of the plume rather than background air. This was done by taking the minimum SO_2 value between peaks from drone flights (1.3 ppmv or 3.3 mg m^{-3}) as a universal background threshold; all SO_2 data and their corresponding GEM data below this threshold were removed from ground- and drone-based datasets (see Mason et al., 2021). The Drone MultiGas SO_2 sensor is calibrated for the concentration range 0–200 ppmv, but the calibration curve preserves linearity approximately 15 % above the maximum (i.e., ~230 ppmv), hence this is the upper threshold for reliable measurements due to SO_2 sensor saturation. While SO_2 levels in the dense volcanic plume periodically exceeded this threshold on the 12 and 16 Aug drone flights, concentrations were below 230 ppmv in ~95 % of the data, so the effects of potentially unreliable measurements on SO_2 flight averages were considered negligible.

In-plume concentration data for both GEM and SO_2 were determined to be non-normally distributed at a 95 % confidence level on all sampling days ($p \leq 0.008$; Kolmogorov-Smirnov test; SPSS Statistics, v.29.0; IBM, Armonk, NY, USA). In order to obtain standard deviations for GEM and SO_2 concentrations on each day, data were resampled by calculating the medians of smaller subsets of data ($n = 10$) representing 100 s of measurements; the mean ± 1 standard deviation (SD) of the resampled subsets were calculated for each gas on a given sampling run with subset N values ranging from 6 to 37 based on the amount of volcanic plume intercepted by the sampling instruments. The data processing procedure is described graphically in Fig. S1.

Subset means were used to calculate mass ratios of GEM and TGM (for ground- and drone-based data, respectively) to SO_2. In the case of the drone-based measurements, the single TGM data point was combined with mean SO_2 concentrations obtained from the Drone MultiGAS over the concurrent sampling interval (also resampled in the manner described above). Mass ratios were analyzed using dedicated post-processing software (Ratiocalc; Tamburello, 2015) to determine any significant correlations in the peaks of the two signals over periods of at least 5 min of consecutive measurements. Relationships between GEM and SO_2 were tested with linear regressions using resampled SO_2 data binned into stratified quantiles above the 25th, 33rd, 50th, 66th, and 75th percentiles to check for any differences in the GEM/SO_2 relationship with different bulk concentrations of volcanic plume.

Additionally, nonparametric statistical tests were run at a 95 % confidence level to determine any significant differences between sampling days (Independent-Samples Kruskal-Wallis Test with Bonferroni correction for multiple tests), between ground-based and drone-based data and between eruption years (Mann Whitney Rank Sum Test) for GEM/SO_2 mass ratios. These tests were not run separately for GEM and SO_2 data since differences in sampling conditions among the different days (e.g., proximity to the gas source, meteorological conditions), rather than changes in the plume chemistry, are expected to dominate any significant differences in mean concentrations.

3. Results

3.1. Ground-based GEM and SO_2 concentrations and ratios

The results of simultaneous and co-spatial GEM (Lumex) and SO_2 (MultiGAS) ground-based measurements of the Fagradalsfjall eruption plume are shown in Table 1. Plume GEM concentrations ranged from 1.5 to 24 ng m^{-3}, with means for each sampling run spanning 2.8–5.8 ng m^{-3} (medians 2.6–5.4 ng m^{-3}). GEM concentrations on 31 Mar 2021 were significantly lower than for the other days. The good agreement in ground-based Hg concentration values between Lumex and ACT measurement techniques (see Edwards et al., 2023) strongly suggests that ground-based TGM is mostly GEM. Plume SO_2 concentrations ranged from 3.4 to 93 mg m^{-3} with means spanning 7.6–13 mg m^{-3} (medians 0.73–11 mg m^{-3}).

Analyses of the time-series data in Ratiocalc yielded no significant correlations in the GEM and SO_2 data (Fig. 3), with GEM concentrations typically drifting from ~2–5 ng m^{-3} with little correlation to SO_2 peaks; the reasons for this are explored in Section 5. There were also no significant correlations between GEM and other major gases (CO_2, H_2S). Linear regression analyses found a significant relationship between time-matched GEM and SO_2 data for 12 Aug 2022 only ($r = 0.24$; $p \leq 0.047$; Table S2); relationships for the other four sampling days were non-significant across all of the SO_2 quantiles ($p > 0.10$). With the lack of consistent GEM/SO_2 correlations, we therefore estimated mass ratios from analyses of the concentration data (mean ± SD) over the relatively

Table 1
Simultaneous plume Hg (GEM and TGM) and SO_2 concentrations and calculated mass ratios from ground- and drone-based sampling of the Fagradalsfjall volcanic plume in 2021 and 2022. Ground-based Hg/SO_2 means that do not share the same superscripts differ significantly at $p < 0.05$; N refers to the number of resampled subsets from each GEM/SO_2 dataset (see Section 2.5).

Sampling date	Sampling duration (min)	Approximate distance to source (m)	N	Mean Hg ± SD (ng m^{-3})	Mean SO_2 ± SD (mg m^{-3})	Hg/SO_2 ± SD × 10^{-7}
Ground-based sampling (Hg = GEM)						
31 Mar 2021	60	250	26	2.8 ± 0.53	11 ± 3.0	2.5 ± 0.8[a]
12 Apr 2021	35	500	6	4.7 ± 0.52	7.8 ± 1.7	6.0 ± 0.6[b]
14 Apr 2021	110	150	37	5.8 ± 1.2	9.4 ± 2.0	6.2 ± 0.7[b]
12 Aug 2022	60	250	29	5.2 ± 0.86	13 ± 5.7	4.0 ± 1.2[b]
16 Aug 2022	50	400	7	4.0 ± 0.24	7.6 ± 1.9	5.3 ± 0.6[b]
Group mean ± SD				4.5 ± 1.7	9.8 ± 7.2	4.8 ± 1.8
Drone-based sampling (Hg = TGM)						
12 Aug 2022	97	75	46*	15	237 ± 64	0.63
16 Aug 2022	110	75	47*	12	243 ± 42	0.49
Group mean[†]				14	240	0.56

* N refers to drone-based SO_2 data points only; calculated plume TGM is a single time-averaged data point.
† Note that ± SD is not reported because the number of sampling days = 2.

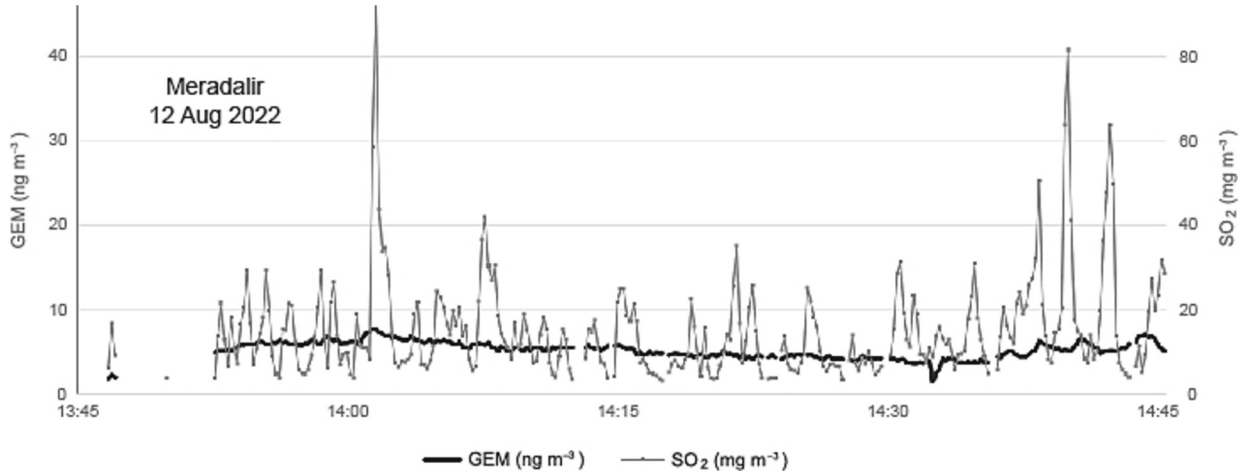

Fig. 3. Simultaneous time-series data of GEM and SO_2 concentrations at 10 s measurement intervals, from 12 Aug 2022 (see Figs. S2 and S3 for time-series plots of the other sampling days). Data gaps represent intervals when the instruments were not sampling the volcanic plume gases due to shifts in wind direction or vertical plume transport away from the sampling location.

long sampling durations, as done in previous studies (e.g., Aiuppa et al., 2007; Witt et al., 2008). These mass ratios ranged from 2.5 to 6.2 × 10^{-7} (group mean 4.8 ± 1.8 × 10^{-7}; $n = 5$).

There were no significant differences between 2021 and 2022 in average GEM ($p = 0.11$) or SO_2 concentrations ($p = 0.17$). The 31 Mar 2021 GEM/SO_2 data were significantly different from the other four sampling days ($p < 0.001$); no significant differences existed among the other days (12 and 14 Apr 2021, 12 and 16 Aug 2022).

3.2. Drone-based Hg and SO_2 concentrations and ratios

In the concentrated near-source plume at Meradalir, TGM concentrations from the drone-mounted ACT sampler were 15 and 12 ng m^{-3} on 12 and 16 Aug 2022, respectively (Table 1). Mean in-plume SO_2 concentrations measured by the Drone MultiGAS over the same sampling period were 237 ± 64 and 243 ± 42 mg m^{-3}, respectively. On 21 Aug 2022, after the eruption had ceased, TGM was 1.7 ng m^{-3} and mean SO_2 was 0.20 ± 0.18 mg m^{-3}. The mean TGM/SO_2 mass ratio from the Aug 12 and 16 flight days was 5.6 × 10^{-8}, one order of magnitude lower and significantly different from the ground-based GEM/SO_2 mass ratios (4.8 ± 1.8 × 10^{-7}; $p = 0.053$; $n = 7$). Analyses of secondary sorbent trap segments yielded small amounts of TGM break-through, ranging from < MDL to 8 % of primary trap TGM (Table S3), and analyses of glass wool yielded no detectable Hg.

The drone-mounted filter pack sample from 6 April 2021 yielded a PBM concentration of 1.7 ng m^{-3}, and simultaneous Drone MultiGAS measurements yielded a mean SO_2 concentration of 127 mg m^{-3} during the 45 min cumulative flight time, yielding a PBM/SO_2 ratio of 1.3 × 10^{-8}. Field blank filters from TGM and PBM sampling flights were all < MDL ($n = 5$).

4. Discussion

While previous studies have collected atmospheric Hg data by drone-mounted instruments above other types of Hg point sources (Black et al., 2018; Cabassi et al., 2022), these are the first reported drone-based volcanic Hg measurements above an actively degassing eruptive vent. Given that much of the available volcanic Hg data in the literature is obtained from ground-based sampling at some distance from the source vent, the near-source data reported here are among the most representative of source plume Hg concentrations from any degassing volcanic system measured to date. Below, we discuss trends in Hg and SO_2 concentrations and corresponding Hg/SO_2 mass ratios measured from near-source aloft to downwind ground-based locations, and contrast the Fagradalsfjall results with other volcanic systems. As a note to the reader, although our ground- and drone-based data represent different Hg fractions as shown in Table 1 (GEM and TGM, respectively), we hereafter refer to all atmospheric gaseous Hg as GEM, since previous work at the site has identified GEM as the dominant Hg form in this environment (Edwards et al., 2023).

4.1. Differences in drone- vs. ground-based Hg/SO_2 mass ratios

Drone-based Hg concentrations measured on the two flight days at Meradalir 2022 (mean 14 ng m^{-3}) represent near-source, high-concentration volcanic plume with a plume aging time (i.e., time from vent emission to measurement) of seconds. Simultaneous ground-based Hg concentrations (mean 4.6 ng m^{-3}) a few hundred meters downwind on the same days (Aug 12 and 16) represent plume aging of 1–2 min based on local wind speeds of ~5 m s^{-1} on both sampling days, and were approximately three-fold lower than the near-source concentrations. These ground-based concentration data were not significantly different from those measured at Geldingadalir in 2021 (mean 4.3 ng m^{-3}). Ground-based SO_2 in 2022 (mean 10.3 mg m^{-3}) was approximately 23-fold lower than drone-based SO_2 (mean 240 mg m^{-3}). Because of an apparently divergent trend in Hg and SO_2 concentrations between near-source aerial and downwind ground-based locations, the mean Hg/SO_2 mass ratios at these locations were significantly different by an order of magnitude (4.8 × 10^{-7} and 5.6 × 10^{-8}, respectively).

However, this difference can be explained by the relative contributions of atmospheric background concentrations of each gas species to their measured concentrations in the active plume. In the ambient atmosphere, SO_2 occurs in trace amounts (< 5 μg m^{-3}; Carmichael et al., 2003; Ilyinskaya et al., 2017) and is typically below the detection limit of volcanic gas monitoring instruments (Galle et al., 2020; Mason et al., 2021). At Fagradalsfjall, the background contribution to measured plume SO_2 is therefore insignificant (< 0.01 %). While background Hg concentrations in the Northern Hemisphere are 1.3–1.5 ng m^{-3} (Driscoll et al., 2013; Sprovieri et al., 2016), we observed an elevated average background concentration near the Fagradalsfjall volcano of 4.0 ng m^{-3}, as determined from measurements made at locations well out of the plume, hundreds of meters from the active vents (Table 2). Similarly elevated local background Hg levels have been observed previously around other volcanoes (4.0–35 ng m^{-3}; Bagnato et al., 2013; Mather et al., 2012; Witt et al., 2008).

At Fagradalsfjall, the source of this elevated background Hg is likely the outgassing lava fields around the active vents, as suggested by two lines of evidence. First, analyses of major gas ratios from the

Table 2
Summary of local background (non-plume) Hg data from the Fagradalsfjall eruption site; 2021 data are from Edwards et al. (2023).

Date	Description and location	Sampling duration (min)	GEM range (ng m^{-3})	GEM mean ± SD (ng m^{-3})
28 Mar 2021	Car traverse beneath plume, ~3 km downwind	35	2.9–6.0	4.2 ± 0.6
13 Apr 2021	~200 m from vent system #5, out of plume	110	1.3–6.3	3.8 ± 0.8
12 Aug 2022	~400 m from Meradalir main vent, out of plume	60	1.4–5.6	3.5 ± 0.9
14 Aug 2022	~200 m from Meradalir main vent, out of plume	255	1.7–7.5	4.2 ± 1.0
Group mean ± SD				4.0 ± 1.7

corresponding MultiGAS datasets for each sampling period showed that lava field emissions, rather than primary vent emissions, dominated the measured ground-based gas, with higher mass ratios of H_2O/SO_2, H_2O/CO_2 and CO_2/SO_2 compared to the drone-based data (Table S1). Second, elevated Hg concentrations (5.0–19 ng m^{-3}) were measured in the near-source fumes of an outgassing lava field at the bottom of Meradalir valley in 2021, isolated from any vent plume contributions (Edwards et al., 2023). This suggests extended degassing of Hg from the cooling lava fields well after the SO_2 has been mainly lost (Thordarson et al., 2003). SO_2 does continue to outgas from the cooling lava, but in significantly lower amounts than the primary vent emissions (Simmons et al., 2017). However, there is a lack of research on the solubility of Hg in basaltic lavas and the dynamics of its outgassing from lava flows compared to main vent emissions. Halogens (Cl, F, Br) are an important volcanic emission product and are known to facilitate the transition of trace metals such as Hg from melt to vapor through metal halide complexation (Hinkley et al., 1994; Mandon et al., 2019). Higher concentrations of halogens relative to SO_2 in the Meradalir lava field emissions may explain the enhanced degassing of Hg from the lava fields relative to SO_2, but further investigations are required. Other possible sources of the elevated local Hg concentrations include enhanced soil Hg degassing from shallow crustal deposits heated by the magmatic dike intrusion, or the re-emission of Hg from burning vegetation impacted by the lava flows.

Regardless of the exact mechanisms at work, the local Hg background contribution of 4.0 ng m^{-3} is considerable when compared to the total ground-based Hg measured, accounting for 77 % of this total on 12 Aug (5.2 ng m^{-3}) approximately 250 m from the eruption vent, and 100 % on 16 Aug (4.0 ng m^{-3}) at 400 m distance. The average Hg attributable to the dilute vent plume (i.e., background-corrected) for both days is 0.6 ng m^{-3}—a concentration so low that it is difficult to resolve above the background signal. This explains the fairly consistent ground-based Hg concentrations over time shown in Fig. 3, which were not significantly correlated with SO_2 peaks as more concentrated parts of the volcanic plume wafted over the sampling location.

Incorporating the average background-corrected plume Hg concentration into the corresponding ground-based Hg/SO_2 calculation (Hg = 0.6 ng m^{-3}; SO_2 = 10.3 mg m^{-3}; averaged between 12 and 16 Aug) yields a mass ratio of 5.8×10^{-8}, which agrees with the mean Hg/SO_2 measured by drone (5.6×10^{-8}; Fig. 4a). This suggests that Hg/SO_2 mass ratios remain fairly conservative in the plume, at least over several hundred meters. This is an important finding given that reported "near-source" plume measurements can take place at widely different distances to the source (from tens of meters to a few km), based on the volcanic site and instrumentation involved in the study (Edwards et al., 2021). If Hg/SO_2 does not vary significantly over the near-source distance involved in many of these measurements (i.e., several hundred meters) as suggested by our results, then this validates the use of the Hg/SO_2 method to estimate volcanic Hg fluxes. Future research attempting to confirm this should ensure that measurements of the primary volcanic plume are not contaminated by lava field outgassing, since the background correction method used above can introduce additional uncertainties.

It should be noted that the mean Hg concentration on 31 Mar 2021

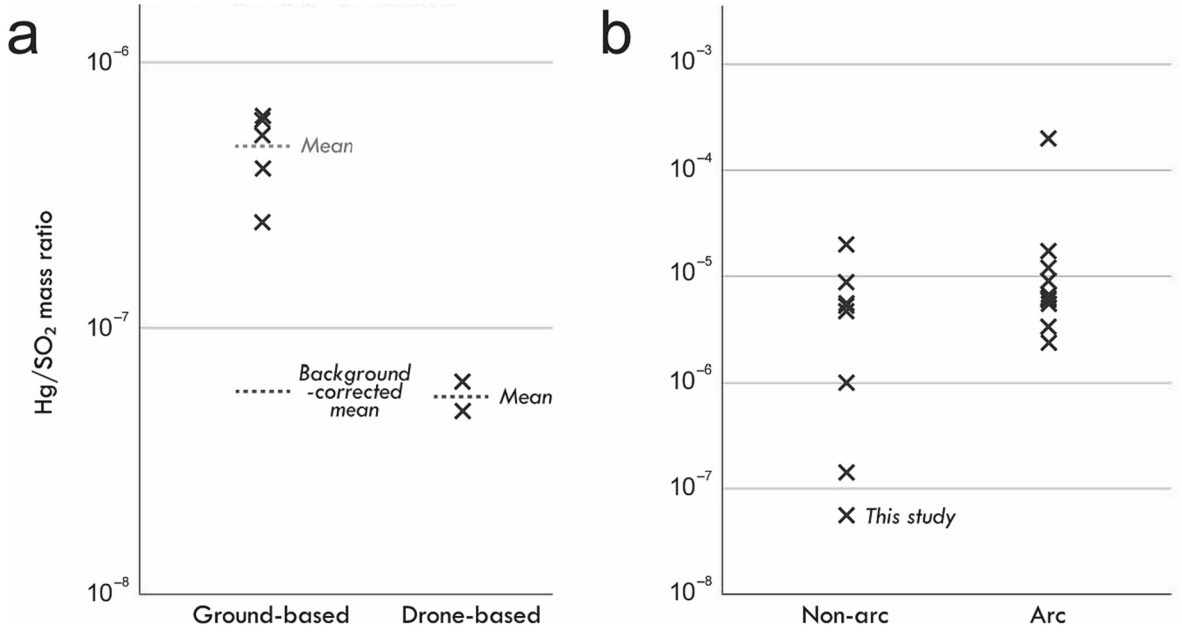

Fig. 4. (**a**) Ground- and drone-based Hg/SO_2 mass ratios from different sampling days at Fagradalsfjall, with raw and background-corrected means indicated; (**b**) literature Hg/SO_2 mass ratios from open-conduit degassing of non-arc (hotspot, rift, composite) and arc volcanoes since the year 2000, including the mass ratio reported in this study.
(Data sources: Allard et al. (2016); Bagnato et al. (2007, 2011, 2014); Ferrara et al. (2000); Friedli et al. (2004); Mather et al. (2012); Schiavo et al. (2020); Wardell et al. (2008).)

(2.8 ng m^{-3}) is lower than the above-cited elevated background concentration of 4.0 ng m^{-3}, and is significantly different from mean concentrations on the other ground-based sampling days. However, this value is still within the standard deviation of the average elevated background (± 1.7 ng m^{-3}; Table 2). Furthermore, a longer timeframe dataset for the same sampling run, but without full SO_2 data coverage, yielded a mean value of 4.9 ng m^{-3} (see Edwards et al., 2023, Supplementary Material Table S1), which agrees with the other ground-based datasets. This may indicate the 60-min sampling interval used here was biased low, likely due to short-term fluctuations in Hg concentrations due to variable background air mixing and plume concentrations.

The above discussion assumes the drone-based TGM sampler captured all gaseous volcanic Hg species. The reliability of activated carbon traps for gaseous Hg sampling has been demonstrated previously at the Fagradalsfjall site (Edwards et al., 2023) and in higher SO_2 industrial flue gas environments (Ghorishi et al., 2002; Huang et al., 2019). Theoretically, some PBM could evade collection on the ACT particulate filter, which captures particles with a minimum diameter of approximately 8.0 μm. This would mean our reported Hg concentrations were biased low. However, rapid post-emission conversion of GEM to PBM within the short timeframe required here (a few seconds) is unlikely, due to GEM's prevalence in the reducing conditions of near-vent plumes and its high vapor pressure (Prestbo and Bloom, 1995; Martin et al., 2011). Previous measurements of similar ash-poor volcanic plumes (e.g., Bagnato et al., 2007; Witt et al., 2008) and the results of geochemical modelling (Martin et al., 2011; Surl et al., 2021; Von Glasow, 2010) support the supposition that GEM is the dominant Hg species near the vent source. The conversion of gaseous Hg (especially GOM) to PBM would instead be expected to occur further downwind, as the volcanic plume cools and Hg condenses onto particulates (Bagnato et al., 2007; Von Glasow, 2010).

Evidence of this later conversion is seen in our single PBM concentration data point, collected 2 km from the eruption in 2021 (1.7 ng m^{-3}), which is orders of magnitude higher than typical background PBM levels (low pg m^{-3}; Kim et al., 2012; Poissant et al., 2005; Swartzendruber et al., 2006). While this was the only PBM value that could be obtained during this study, the resulting PBM/SO_2 ratio (1.3×10^{-8}) suggests a ~ 25 % conversion of TGM to PBM over the 2 km distance based on the near-source TGM/SO_2 ratio in the volcanic plume (5.6×10^{-8}), assuming total plume Hg is conserved. However, we caution that in the absence of concurrent TGM measurements from this drone flight, and hence a full picture of downwind Hg speciation, this is a highly speculative estimate. It is nevertheless worth noting that this speciation agrees with the results of geochemical plume modelling by Von Glasow (2010), where 25 % of plume Hg existed as PBM at a plume aging time of ~5 min, which is approximately the time taken for the Fagradalsfjall plume to traverse the 2 km distance in this case (assuming an average wind speed of 5 m s^{-1}).

4.2. Estimated Hg flux from Fagradalsfjall volcano, 2021 and 2022

Fagradalsfjall was an exceptionally low Hg source compared to other open-conduit active volcanoes. The average background-corrected Hg concentration measured by drone (10 ng m^{-3}) is lower than those (uncorrected) concentrations in the plumes of other hotspot/rift and arc volcanoes (Table 3), even though our data likely represents the closest Hg measurements taken near an active volcanic vent. For comparison, Bagnato et al. (2007) sampled the plume of Etna from a comparable distance (< 100 m), finding average concentrations of 277 ng m^{-3}. Our ground-based data at several hundred meters distance were only slightly above background ambient levels.

For estimating total Hg emissions from Fagradalsfjall, we use the Hg/SO_2 mass ratio calculated from drone-based measurements of the more concentrated plume. Although the instrumental uncertainties estimated above for the drone-based sampling configuration (~20 %) are higher than the ground-based Lumex instrument (~10 %), we note that gas sampled closer to the source will have an enhanced signal-to-noise ratio (and thus a lower uncertainty) compared to downwind measurements due to the effects of background air dilution (Liu et al., 2020).

Table 3
Summary of gaseous Hg concentrations in volcanic plumes and corresponding Hg/SO_2 mass ratios from measurements made within a few hundred meters of the active vents of several hotspot/rift and arc volcanoes; values are averaged from data reported in the corresponding references.

Volcano	Country	Tectonic setting	Mean Hg (ng m^{-3})	Hg/SO_2	Reference
Etna	Italy	Composite	195	5.3×10^{-7}	Bagnato et al. (2007, 2014)
Masaya	Nicaragua	Arc	164	2.0×10^{-5}	Witt et al. (2008)
Ambrym	Vanuatu	Arc	124	7.7×10^{-6}	Allard et al. (2016), Bagnato et al. (2011)
Turrialba	Costa Rica	Arc	99	5.9×10^{-6}	Bagnato et al. (2014)
Miyake-jima	Japan	Arc	95	5.7×10^{-6}	Bagnato et al. (2011), Friedli et al. (2004)
Asama	Japan	Arc	41	5.5×10^{-6}	Bagnato et al. (2011)
Nyiragongo	DRC	Hotspot/rift	373	5.5×10^{-6}	Bagnato et al. (2011)
Kīlauea	USA	Hotspot/rift	35	1.6×10^{-6}	Mather et al. (2012)
Fagradalsfjall	Iceland	Hotspot/rift	10	5.6×10^{-8}	This work

Combining the near-source Hg/SO_2 mass ratio (5.6×10^{-8}) with the average total SO_2 emissions from the 2021 eruption (0.74 ± 0.59 Mt.; Barsotti et al., 2023; Esse et al., 2023), we estimate a cumulative emitted Hg mass from Fagradalsfjall of 46 ± 33 kg over the 200 eruptive days in 2021 and 2022, equivalent to a flux of 0.23 ± 0.17 kg d^{-1} or 0.08 ± 0.06 t a^{-1}. We note that this estimate encompasses several distinct phases of variable lava and gas output when no Hg measurements were made (Barsotti et al., 2023) and therefore assumes Hg/SO_2 does not vary significantly throughout the eruption. However, the lack of significant differences in mean Hg/SO_2 among four of the five sampling days supports the use of a time-averaged flux estimate.

In terms of other reported fluxes in the volcanic Hg literature, our estimate is slightly below the range for other open-conduit rift/hotspot volcanoes (0.60–12 kg d^{-1}; Fig. 5), which is consistent with the fact that volcanoes generally exhibit Hg/SO_2 values (10^{-6}–10^{-5}) that are 2–3 orders of magnitude higher than Fagradalsfjall; Hg/SO_2 values for other active rift/hotspot volcanoes such as Kīlauea (Mather et al., 2012) and Nyiragongo (Bagnato et al., 2011) average ~ 10^{-6} (Fig. 4b). Compared to rift/hotspot systems, Hg fluxes from subduction-zone arc volcanoes are generally higher (0.5–110 kg d^{-1}), with several being one or two orders of magnitude higher, such as Ambrym (49–74 kg d^{-1}; Allard et al., 2016; Bagnato et al., 2011), Miyake-jima (18–61 kg d^{-1}; Bagnato et al., 2011; Friedli et al., 2004), Popocatépetl (9.8–110 kg d^{-1}; Goff et al., 1998; Schiavo et al., 2020), and Masaya (19 kg d^{-1}; Witt et al., 2008).

4.3. Implications for volcanic Hg degassing

The apparent distinction in volcanic Hg emissions between arc and hotspot/rift volcanoes has been noted elsewhere (Bagnato et al., 2011, 2014; Edwards et al., 2021). However, the dominance of arc volcanism in the global Hg emissions dataset, and the reciprocal lack of data for hotspot/rift systems, makes it difficult to draw conclusions regarding the sources and mechanisms of Hg release from these two endmember geotectonic settings. Nevertheless, some inferences can be made about the relative amounts of Hg contained within the different geological

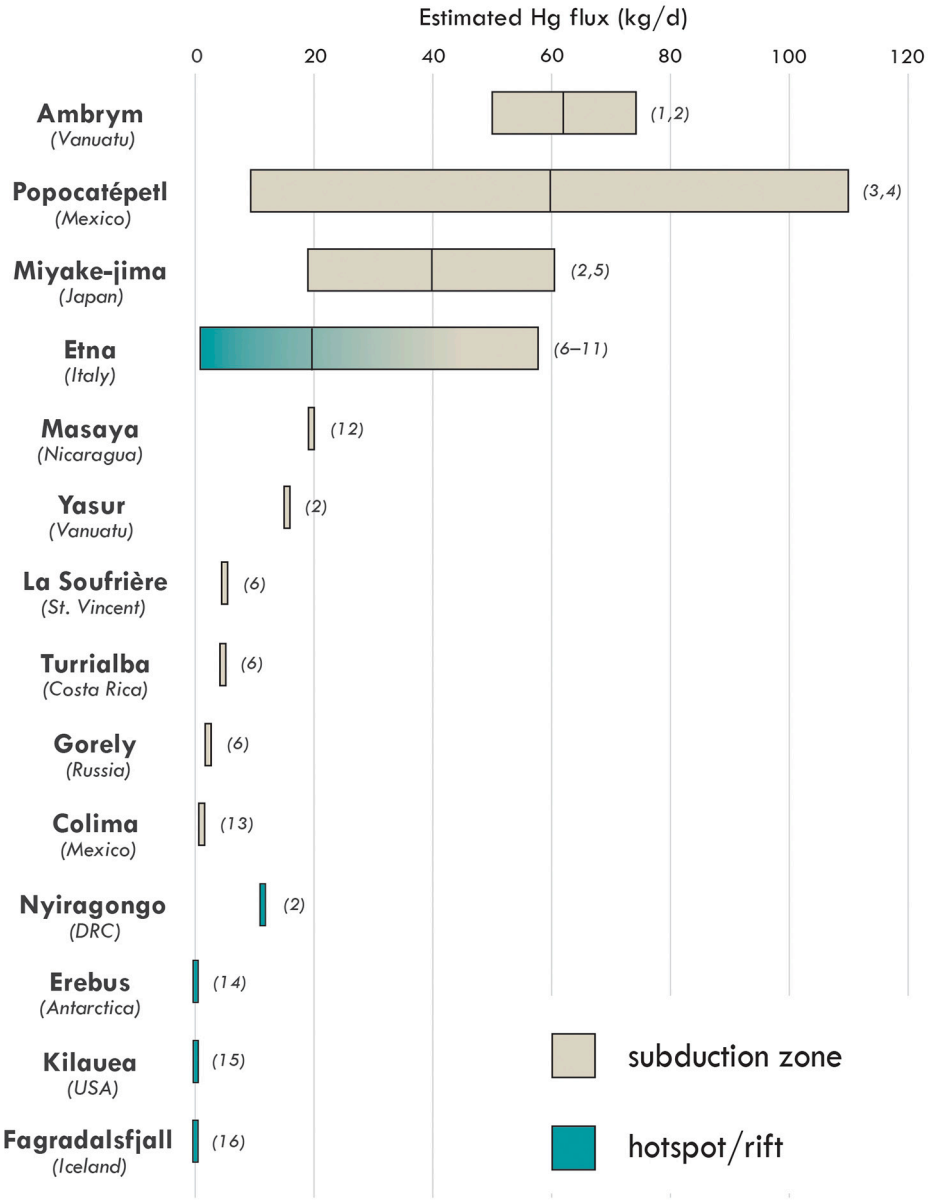

Fig. 5. Mercury flux estimates for Fagradalsfjall compared with reported values for subduction-zone arc, composite and hotspot/rift volcanic systems. Vertical bars within the boxes represent the mean of multiple data sources. Etna is generally classified as a composite arc/hotspot system, hence its box's dual shading. (Data sources: [1]Allard et al. (2016); [2]Bagnato et al. (2011); [3]Goff et al. (1998); [4]Schiavo et al. (2020); [5]Friedli et al. (2004); [6]Bagnato et al. (2014); [7]Calabrese et al. (2011); [8]Bagnato et al. (2007); [9]Ferrara et al. (2000); [10]Ferrara and Maserti (1990); [11]Dedeurwaerder et al. (1982); [12]Witt et al. (2008); [13]Varekamp and Buseck (1986); [14]Wardell et al. (2008); [15]Mather et al. (2012); [16]This work.)

reservoirs from which these settings are typically sourced.

The Fagradalsfjall eruptions tapped relatively deep magmas from 15 to 20 km depth directly (Halldórsson et al., 2022; Krmíček et al., 2022), rather than a shallow magma chamber where intermediate processes (e.g., assimilation of Hg-rich crustal material) may greatly alter magma composition. The surface plume sampled in this work therefore represents degassing from a fresh batch of depleted mantle which appears to be a particularly low-Hg geological reservoir. Two factors allow us to infer this: 1) the relatively low Hg concentrations measured in the Fagradalsfjall eruption plume, and 2) Hg's relatively high degassing efficiency from basaltic magmas, based on its volatility and the characteristics of other metals with similar geochemical behavior (e.g., Be, Si; Coufalík et al., 2018; Edmonds et al., 2018; Henley and Berger, 2013; Pyle and Mather, 2003). Mercury degassing from basaltic magmas may potentially be hindered by the lower concentrations of halogens (which facilitate Hg transport from melt to vapor) in hotspot/rift magmas compared to their subduction-zone arc counterparts (Edmonds et al., 2018; Gauthier et al., 2016; Hinkley et al., 1999). However, analyses of ultramafic rocks such as peridotites suggest low Hg concentrations in the source magmas, rather than incomplete degassing, are behind the low observed Hg emissions at the surface. Based on analyses of mantle peridotite xenoliths, upper mantle Hg concentrations are estimated as 0.2–0.4 ng g^{-1} (Canil et al., 2015; Coufalík et al., 2018). Both Coderre and Steinthorsson (1977) and Bagnato et al. (2018) report average basalt Hg concentrations of 3 ng g^{-1} in Iceland and the volcanic rift setting of the Azores, respectively. In contrast, magma from Etna, a complex geotectonic system with arc-like characteristics, is estimated to contain 20–60 ng g^{-1} Hg (Aiuppa et al., 2003; Pyle and Mather, 2003). While this could indicate a naturally high Hg content in the local mantle source, it could also be due to secondary crustal contamination processes; e.g., Hg release during wall-rock assimilation by magma bodies of crustal materials such as epithermal deposits (Canil et al., 2015; Gao

et al., 2022). The crust is a more enriched Hg reservoir than the mantle, with concentrations ranging from 5 to 160 ng g^{-1} worldwide, and zones of Hg mineral deposits formed through mantle degassing processes occur along much of the Earth's plate boundaries (known as "mercuriferous belts"; Agnan et al., 2016; Rytuba, 2003). These belts can contain Hg deposits with concentrations exceeding 50 μg g^{-1} (Gustin et al., 2000). In regions such as Mexico, Vanuatu, and Japan, the coincidence of Hg-enriched zones and modern day subduction-zone arc volcanism suggests a crustal origin for the higher Hg emissions seen at volcanoes in these regions (e.g., Popocatépetl, Ambrym, Miyake-jima). Similarly, the massive Hg-enriched belt that traverses the Mediterranean, and which historically sustained large Hg mining regions in Spain and Italy (Rimondi et al., 2015), is implicated in the elevated Hg degassing at Etna.

The results of this field study lend additional evidence to the argument that hotspot/rift volcanoes are minor Hg emitters in general, and add an important additional piece to the puzzle of global volcanic Hg degassing. However, further data from other hotspot/rift volcanic systems, especially during active eruptions, is required before further discussion of the implications for the global volcanic Hg flux is justified. At the same time, these efforts should be balanced with further field campaigns at arc volcanoes, which appear to be more important Hg sources overall.

4.4. The future of volcanic Hg gas sampling

In the volcanic gas community, drone-based sampling of plume gases and particulates has been the preferred approach for several years now, offering greater access to near-source plumes "uncontaminated" by background air, while reducing the risks for scientists on the ground (James et al., 2020). Recently, researchers have leveraged increasingly compact and reliable drone-mounted instruments and longer flight durations to obtain high-quality volcanic plume measurements of major gases and aerosols (e.g., D'Arcy et al., 2022; De Moor et al., 2019; McGonigle et al., 2008; Galle et al., 2020; Liu et al., 2019), particulate material (e.g., Mason et al., 2021; Mori et al., 2016; Stix et al., 2018), and a suite of volatile and refractory trace metals (e.g., Mandon et al., 2019; Mason et al., 2021) which have not previously included Hg.

In this study we have shown that sampling of volcanic Hg very close to an active vent is now feasible with drone-based instruments specifically designed for Hg collection. Future sampling of plume Hg species should prioritize such aerial sampling techniques to better understand near-source as well as downwind plume Hg concentrations and speciation; in particular, interconversions among GEM, GOM and PBM compounds, and the behavior of Hg and other major gases with atmospheric mixing and dilution as the plume ages. This will allow for the ground-truthing of plume Hg modelling studies that hold important implications for the depositional trends and environmental fate of volcanic Hg (e.g., Surl et al., 2021; Von Glasow, 2010) and provide insight into the conservative nature of Hg/SO_2 mass ratios in plumes. To sample all Hg species (TGM and PBM), we recommend a dedicated PBM sampling device in addition to the ACT sampler, such as the 1.0-μm filter pack setup used in our 2021 field campaign. The different flow rates required for each sampler (1–3 L min^{-1} for TGM; tens to hundreds L min^{-1} for PBM) would likely necessitate the use of separate air pumps, increasing payload. This issue could be avoided by attaching a flow splitter to the higher volume pump with a flow rate controller or throttle to reduce air flow in the TGM sampling line to an optimal flow rate. To quantify ACT sampling precision, a separate flow splitter attached to the ACT sampling line would permit simultaneous sampling on multiple replicate sorbent traps with little additional payload (e.g., Black et al., 2018).

Our work also shows the importance of accounting for atmospheric background Hg when interpreting volcanic plume data. While this is routinely done for volcanic CO_2 measurements because of the significant background CO_2 concentration (e.g., Shinohara et al., 2008; Werner et al., 2006), it has not usually been done for Hg, likely because previous reported plume Hg concentrations are typically in the range of many tens to hundreds of ng m^{-3}. At Hg-poor systems such as Fagradalsfjall, or at distant locations where atmospheric mixing has diluted the Hg concentration signal to near-ambient levels (e.g., Schiavo et al., 2020), background concentrations may comprise a large fraction of measured plume Hg. Therefore, in specific cases it may be best practice to remove this background fraction from reported data and calculated Hg/SO_2 mass ratios.

CRediT authorship contribution statement

Brock A. Edwards: Writing – review & editing, Writing – original draft, Visualization, Methodology, Investigation, Formal analysis, Data curation, Conceptualization. **Melissa A. Pfeffer:** Writing – review & editing, Investigation, Formal analysis. **Evgenia Ilyinskaya:** Writing – review & editing, Investigation. **Barbara I. Kleine-Marshall:** Writing – review & editing, Investigation. **Céline L. Mandon:** Writing – review & editing, Investigation. **Adam Cotterill:** Writing – review & editing, Investigation. **Alessandro Aiuppa:** Writing – review & editing, Visualization, Investigation. **Peter M. Outridge:** Writing – review & editing, Supervision, Methodology, Investigation, Funding acquisition, Formal analysis, Conceptualization. **Feiyue Wang:** Writing – review & editing, Validation, Supervision, Resources, Project administration, Methodology, Investigation, Funding acquisition, Formal analysis, Data curation, Conceptualization.

Declaration of competing interest

The authors declare that they have no known competing financial interests or personal relationships that could have appeared to influence the work reported in this paper.

Data availability

Data are available through the Canadian Watershed Information Network (CanWIN) data repository at https://doi.org/10.34992/pnqh-zs42.

Acknowledgements

This work was supported by funding from the Geological Survey of Canada (Environmental Geosciences Program), the Natural Sciences and Research Council of Canada, the Canada Research Chairs Program and the UK Natural Environment Research Council Centre for the Observation & Modelling of Earthquakes, Volcanoes & Tectonics (NERC COMET+). Field assistance was graciously provided by the Icelandic Meteorological Office, the University of Iceland and Iceland Search and Rescue (Björgunarsveit). In particular, we acknowledge Samuel Scott, Sibylle von Löwis of Menar, Elísabet Pálmadóttir, Tryggvi Hjörvar, Ríkey Kjartansdóttir, Esther Hlíðar Jensen, Ásta Rut Hjartardóttir, Gerður Stefánsdóttir, Baldur Bergsson, Hermann Arngrímsson and Andri Stefánsson. The Svarmi drone team of Kordian Skwarczek, Sydney Gunnarson, Daniel Ben-Yehoshua and Tryggvi Stefánsson are thanked for their expert flight operations in challenging conditions. We would also like to thank Debbie Armstrong, Laura Wainman, Yanique Campbell, Marcello Bitetto, Artem Egorov and Diego Salgado-Sanchez for technical support, and Zhiyuan (Jeff) Gao and Skye Kushner for helpful discussions during the writing of this manuscript.

Appendix A. Supplementary material

Supplementary material includes ground-based and aerial drone-based measurements of mercury and major gases at the Fagradalsfjall eruption site (**Table S1**), graphical illustration of GEM and SO_2 data processing procedure (**Fig. S1**), regression analyses for stratified quantiles above the five SO_2 concentration percentiles (**Table S2**), data from

analyses of drone-based ACT samples from the 2022 campaign (**Table S3**), and time-series data of simultaneous GEM and SO_2 concentrations at Geldingadalir in 2021 (**Fig. S2**) and at Meradalir in 2022 (**Fig. S3**).

References

Agnan, Y., Le Dantec, T., Moore, C.W., Edwards, G.C., Obrist, D., 2016. New constraints on terrestrial surface–atmosphere fluxes of gaseous elemental mercury using a global database. Environ. Sci. Technol. 50, 507–524.

Aiuppa, A., Dongarrà, G., Valenza, M., 2003. Degassing of trace volatile metals during the 2001 eruption of Etna. In: Robock, A., Oppenheimer, C. (Eds.), Volcanism and the Earth's Atmosphere, 139. American Geophysical Union, pp. 41–54.

Aiuppa, A., Federico, C., Giudice, G., Gurrieri, S., 2005. Chemical mapping of a fumarolic field: La Fossa Crater, Vulcano Island (Aeolian Islands, Italy). Geophys. Res. Lett. 32, L13309.

Aiuppa, A., Bagnato, E., Witt, M.L.I., Mather, T.A., Parello, F., Pyle, D.M., Martin, R.S., 2007. Real-time simultaneous detection of volcanic hg and SO_2 at La Fossa Crater, Vulcano (Aeolian Islands, Sicily). Geophys. Res. Lett. 34, L21307.

Aiuppa, A., Bertagnini, A., Métrich, N., Moretti, R., Di Muro, A., Liuzzo, M., Tamburello, G., 2010. A model of degassing for Stromboli volcano. Earth Planet. Sci. Lett. 295, 195–204.

Allard, P., Aiuppa, A., Bani, P., Metrich, N., Bertagnini, A., Gauthier, P.J., Shinohara, H., Sawyer, G., Parello, F., Bagnato, E., Pelletier, B., Garaebiti, E., 2016. Prodigious emission rates and magma degassing budget of major, trace and radioactive volatile species from Ambrym basaltic volcano, Vanuatu island Arc. J. Volcanol. Geotherm. Res. 322, 119–143.

AMAP/UNEP, 2019. Technical background report for the global mercury assessment 2018. In: Arctic Monitoring and Assessment Programme, Oslo, Norway/UN Environment Programme, Chemicals and Health Branch, Geneva, Switzerland viii + 426 pp.

Arnórsson, S., 1995. Geothermal systems in Iceland: structure and conceptual models—I. High-temperature areas. Geothermics 24, 561–602.

Bagnato, E., Aiuppa, A., Parello, F., Calabrese, S., D'Alessandro, W., Mather, T.A., McGonigle, A.J.S., Pyle, D.M., Wangberg, I., 2007. Degassing of gaseous (elemental and reactive) and particulate mercury from Mount Etna volcano (Southern Italy). Atmos. Environ. 41, 7377–7388.

Bagnato, E., Aiuppa, A., Parello, F., Allard, P., Shinohara, H., Liuzzo, M., Giudice, G., 2011. New clues on the contribution of Earth's volcanism to the global mercury cycle. Bull. Volcanol. 73, 497–510.

Bagnato, E., Tamburello, G., Aiuppa, A., Sprovieri, M., Vougioukalakis, G.E., Parks, M., 2013. Mercury emissions from soils and fumaroles of Nea Kameni volcanic centre, Santorini (Greece). Geochem. J. 47, 437–450.

Bagnato, E., Tamburello, G., Avard, G., Martinez-Cruz, M., Enrico, M., Fu, X., Sprovieri, M., Sonke, J.E., 2014. Mercury fluxes from volcanic and geothermal sources: an update. Geol. Soc. Lond. Spec. Publ. 410, 263–285.

Bagnato, E., Viveiros, F., Pacheco, J.E., D'Agostino, F., Silva, C., Zanon, V., 2018. Hg and CO_2 emissions from soil diffuse degassing and fumaroles at Furnas Volcano (Sao Miguel Island, Azores): gas flux and thermal energy output. J. Geochem. Explor. 190, 39–57.

Barsotti, S., Parks, M.M., Pfeffer, M.A., Óladóttir, B.A., Barnie, T., Titos, M.M., Jónsdóttir, K., Pedersen, G.B.M., Hjardardóttir, Á.R., Stefansdóttir, G., Jóhannsson, T., Arason, T., Gudmundsson, M.T., Oddsson, B., Þrastarson, R.H., Ófeigsson, B.G., Vogfjörd, K., Geirsson, H., Hjörvar, T., von Löwis, S., Pedersen, G.N., Sigurðsson, E.M., 2023. The eruption in Fagradalsfjall (2021, Iceland): how the operational monitoring and the volcanic hazard assessment contributed to its safe access. Nat. Hazards 116, 3063–3092.

Black, O., Chen, J., Scircle, A., Zhou, Y., Cizdziel, J.V., 2018. Adaption and use of a quadcopter for targeted sampling of gaseous mercury in the atmosphere. Environ. Sci. Pollut. Res. 25, 13195–13202.

Cabassi, J., Lazzaroni, M., Giannini, L., Mariottini, D., Nisi, B., Rappuoli, D., Vaselli, O., 2022. Continuous and near real-time measurements of gaseous elemental mercury (GEM) from an unmanned aerial vehicle: a new approach to investigate the 3D distribution of GEM in the lower atmosphere. Chemosphere 288, 132547.

Calabrese, S., Aiuppa, A., Allard, P., Bagnato, E., Bellomo, S., Brusca, L., D'Alessandro, W., Parello, F., 2011. Atmospheric sources and sinks of volcanogenic elements in a basaltic volcano (Etna, Italy). Geochim. Cosmochim. Acta 75, 7401–7425.

Canil, D., Crockford, P.W., Rossin, R., Telmer, K., 2015. Mercury in some arc crustal rocks and mantle peridotites and relevance to the moderately volatile element budget of the Earth. Chem. Geol. 396, 134–142.

Carmichael, G.R., Ferm, M., Thongboonchoo, N., Woo, J.-H., Chan, L.Y., Murano, K., Viet, P.H., Mossberg, C., Bala, R., Boonjawat, J., Upatum, P., Mohan, M., Adhikary, S.P., Shrestha, A.B., Pienaar, J.J., Brunke, E.B., Chen, T., Jie, T., Guoan, D., Peng, L. C., Dhiharto, S., Harjanto, H., Jose, A.M., Kimani, W., Kirouane, A., Lacaux, J.-P., Richard, S., Barturen, O., Cerda, J.C., Athayde, A., Tavares, T., Cotrina, J.S., Bilici, E., 2003. Measurements of sulfur dioxide, ozone and ammonia concentrations in Asia, Africa, and South America using passive samplers. Atmos. Environ., 37: 1293e1308.

Coderre, J.A., Steinthorsson, S., 1977. Natural concentrations of mercury in Iceland. Geochim. Cosmochim. Acta 41, 419–424.

Coufalík, P., Krmicek, L., Zverina, O., Meszarosova, N., Hladil, J., Komarek, J., 2018. Model of mercury flux associated with volcanic activity. Bull. Environ. Contam. Toxicol. 101, 554–555.

D'Arcy, F., De Moor, J.M., Stix, J., Alan, A., Bogue, R., Corrales, E., Diaz, J.A., Mick, E., Salas-Navarro, J., Lauzeral, R., 2022. New insights into carbon isotope systematics at Poás volcano, Costa Rica. J. Volcanol. Geotherm. Res. 431, 107639.

De Moor, J.M., Stix, J., Avard, G., Muller, C., Corrales, E., Diaz, J.A., Alan, A., Brenes, J., Pacheco, J., Aiuppa, A., Fischer, T.P., 2019. Insights on hydrothermal-magmatic interactions and eruptive processes at Poás Volcano (Costa Rica) from high-frequency gas monitoring and drone measurements. Geophys. Res. Lett. 46, 1293–1302.

Dedeurwaerder, H., Decadt, G., Baeyens, W., 1982. Estimations of mercury fluxes emitted by Mount Etna volcano. Bull. Volcanol. 45, 191–196.

Driscoll, C.T., Mason, R.P., Chan, H.M., Jacob, D.J., Pirrone, N., 2013. Mercury as a global pollutant: sources, pathways, and effects. Environ. Sci. Technol. 47, 4967–4983.

Edmonds, M., Mather, T.A., Liu, E.J., 2018. A distinct metal fingerprint in arc volcanic emissions. Nat. Geosci. 11, 790–794.

Edwards, B.A., Kushner, D.S., Outridge, P.M., Wang, F., 2021. Fifty years of volcanic mercury emission research: knowledge gaps and future directions. Sci. Total Environ. 757, 143800.

Edwards, B.A., Pfeffer, M.A., Jóhannsson, Þ., Outridge, P.M., Wang, F., 2023. An inter-method comparison of mercury measurements in Icelandic volcanic gases. Appl. Geochem. 152, 105654.

Esse, B., Burton, M., Hayer, C., Pfeffer, M.A., Barsotti, S., Theys, N., Barnie, T., Titos, M., 2023. Satellite derived SO_2 emissions from the relatively low-intensity, effusive 2021 eruption of Fagradalsfjall. Iceland. Earth and Planetary Science Letters 619, 118325.

Ferrara, R., Maserti, B.E., 1990. Atmospheric mercury levels in the Mount Etna volcanic area after an eruptive phase. Environ. Technol. 11, 51–56.

Ferrara, R., Mazzolai, B., Lanzillotta, E., Nucaro, E., Pirrone, N., 2000. Volcanoes as emission sources of atmospheric mercury in the Mediterranean basin. Sci. Total Environ. 259, 115–121.

Fischer, T.P., Chiodini, G., 2015. Volcanic, magmatic and hydrothermal gases. In: Sigurdsson, H., Houghton, B., McNutt, S., Rymer, H., Stix, J. (Eds.), The Encyclopedia of Volcanoes. Elsevier, pp. 779–797.

Friedli, H.R., Radke, L.F., Prescott, R., Li, P., Woo, J.-H., Carmichael, G.R., 2004. Mercury in the atmosphere around Japan, Korea, and China as observed during the 2001 ACE-Asia field campaign: measurements, distributions, sources, and implications. J. Geophys. Res. 109, D19S25.

Galle, B., Arellano, S., Bobrowski, N., Conde, V., Fischer, T.P., Gerdes, G., Gutmann, A., Hoffmann, T., Itikarai, I., Krejci, T., Liu, E.J., Mulina, K., Nowicki, S., Richardson, T., Rüdiger, J., Wood, K., Xu, J., 2020. A multi-purpose, multi-rotor drone system for long-range and high-altitude volcanic gas plume measurements. Atmos. Meas. Tech. 14, 4255–4277.

Gao, L., Long, T.-M., Sun, D., Deng, C., Tian, Z., Song, X.-Y., Yin, R., 2022. Crustal mercury addition into the Giant Jinchuan Ni-Cu sulfide deposit, China, and its geological implications. Geochem. Geophys. Geosyst. 23, e2022GC010349.

Gauthier, P.-J., Sigmarsson, O., Gouhier, M., Haddadi, B., Moune, S., 2016. Elevated gas flux and trace metal degassing from the 2014–2015 fissure eruption at the Bárðarbunga volcanic system, Iceland. J. Geophys. Res. Solid Earth 121, 1610–1630.

Ghorishi, S.B., Keeney, R.M., Serre, S.D., Gullett, K.D., Jozewicz, W.S., 2002. Development of a cl-impregnated activated carbon for entrained-flow capture of elemental mercury. Environ. Sci. Technol. 36, 4454–4459.

Goff, F., Janik, C.J., Delgado, H., Werner, C., Counce, D., Stimac, J.A., Siebe, C., Love, S. P., Williams, S.N., Fischer, T., Johnson, L., 1998. Geochemical surveillance of magmatic volatiles at Popocatepetl volcano, Mexico. Geol. Soc. Am. Bull. 110, 695–710.

Gustin, M.S., Lindberg, S.E., Austin, K., Coolbaugh, M., Vette, M., Zhang, H., 2000. Assessing the contribution of natural sources to regional atmospheric mercury budgets. Sci. Total Environ. 259, 61–71.

Halldórsson, S.A., Marshall, E.W., Caracciolo, A., Matthews, S., Bali, E., Rasmussen, M.B., Ranta, E., Robin, J.G., Guðfinnsson, G.H., Sigmarsson, O., Maclennan, J., Jackson, M.G., Whitehouse, M.J., Jeon, H., van der Meer, Q.H.A., Mibei, G.K., Kalliokoski, M.H., Repczynska, M.M., Rúnarsdóttir, R.H., Sigurðsson, G., Pfeffer, M. A., Scott, S.W., Kjartansdóttir, R., Kleine, B.I., Oppenheimer, C., Aiuppa, A., Ilyinskaya, E., Bitetto, M., Giudice, G., Stefánsson, A., 2022. Rapid shifting of a deep magmatic source at Fagradalsfjall volcano, Iceland. Nature 609, 529–534.

Henley, R.W., Berger, B.R., 2013. Nature's refineries – metals and metalloids in arc volcanoes. Earth Sci. Rev. 125, 146–170.

Hinkley, T.K., Le Cloarec, M.F., Lambert, G., 1994. Fractionation of families of major, minor, and trace metals across the melt-vapor interface in volcanic exhalations. Geochim. Cosmochim. Acta 58, 3255–3263.

Hinkley, T.K., Lamothe, P.J., Wilson, S.A., Finnegan, D.L., Gerlach, T.M., 1999. Metal emissions from Kilauea, and a suggested revision of the estimated worldwide metal output by quiescent degassing of volcanoes. Earth Planet. Sci. Lett. 170, 315–325.

Horowitz, H.M., Jacob, D.J., Zhang, Y., Dibble, T.S., Slemr, F., Amos, H.M., Schmidt, J. A., Corbitt, E.S., Marais, E.A., Sunderland, E.M., 2017. A new mechanism for atmospheric mercury redox chemistry: implications for the global mercury budget. Atmos. Chem. Phys. 17, 6353–6371.

Huang, T., Duan, Y., Luo, Z., Zhao, S., Geng, X., Xu, Y., Huang, Y., Wei, H., Ren, S., Wang, H., Gu, X., 2019. Influence of flue gas conditions on mercury removal by activated carbon injection in a pilot-scale circulating fluidized bed combustion system. Ind. Eng. Chem. Res. 58, 15553–15561.

Ilyinskaya, E., Schmidt, A., Mather, T.A., Pope, F.D., Witham, C., Baxter, P., Jóhannsson, T., Pfeffer, M., Barsotti, S., Singh, A., Sanderson, P., Bergsson, B., Kilbride, B.M., Donovan, A., Peters, N., Oppenheimer, C., Edmonds, M., 2017. Understanding the environmental impacts of large fissure eruptions: aerosol and gas emissions from the 2014–2015 Holuhraun eruption (Iceland). Earth Planet. Sci. Lett. 472, 309–322.

Ilyinskaya, E., Mason, E., Wieser, P.E., Holland, L., Liu, E.J., Mather, T.A., Edmonds, M., Whitty, R.C.W., Elias, T., Nadeau, P.A., Schneider, D.J., McQuaid, J.B., Allen, S.E., Harvey, J., Oppenheimer, C., Kern, C., Damby, D., 2021. Rapid metal pollutant deposition from the volcanic plume of Kīlauea, Hawai'i. Communications Earth & Environment 2, 78.

James, M.R., Carr, B.B., D'Arcy, F., Diefenbach, A.K., Dietterich, H.R., Fornaciai, A., Lev, E., Liu, E.J., Pieri, D.C., Rodgers, M., Smets, B., Terada, A., von Aulock, F.W., Walter, T.R., Wood, K.T., Zorn, E.U., 2020. Volcanological applications of unoccupied aircraft systems (UAS): developments, strategies, and future challenges. Volcanica 3, 67–114.

Kim, P.-R., Han, Y.-J., Holsen, T.M., Yi, S.-M., 2012. Atmospheric particulate mercury: concentrations and size distributions. Atmos. Environ. 61, 94–102.

Krmíček, L., Troll, VR., Galiová, M.V., Thordarson, T., Brabec, M., 2022. Trace element composition in olivine from the 2022 Meradalir eruption of the Fagradalsfjall Fires, SW-Iceland. Czech Polar Reports, 12: 222–231.

Li, C., Sonke, J.E., Le Roux, G., Piotrowska, N., Van der Putten, N., Roberts, S.J., Daley, T., Rice, E., Gehrels, R., Enrico, M., Mauquoy, D., Roland, T.P., De Vleeschouwer, F., 2020. Unequal anthropogenic enrichment of mercury in Earth's northern and southern hemispheres. ACS Earth and Space Chemistry 4, 2073–2081.

Lindberg, S., Bullock, R., Ebinghaus, R., Engstrom, D., Feng, X., Fitzgerald, W., Pirrone, N., Prestbo, E., Seigneur, C., 2007. A synthesis of progress and uncertainties in attributing the sources of mercury in deposition. AMBIO: A Journal of the Human Environment 36, 19–33.

Liu, E.J., Wood, K., Mason, E., Edmonds, M., Aiuppa, A., Giudice, G., Bitetto, M., Francofonte, V., Burrow, S., Richardson, T., Watson, M., Pering, T.D., Wilkes, T.C., McGonigle, A.J.S., Velasquez, G., Melgarejo, C., Bucarey, C., 2019. Dynamics of outgassing and plume transport revealed by proximal unmanned aerial system (UAS) measurements at Volcán Villarrica, Chile. Geochem. Geophys. Geosyst. 20, 730–750.

Liu, E.J., Aiuppa, A., Alan, A., Arellano, S., Bitetto, M., Bobrowski, N., Carn, S., Clarke, R., Corrales, E., De Moor, J.M., Diaz, J.A., Edmonds, M., Fischer, T.P., Freer, J., Fricke, G.M., Galle, B., Gerdes, G., Giudice, G., Gutmann, A., Hayer, C., Itikarai, I., Jones, J., Mason, E., McCormick Kilbride, B.T., Mulina, K., Nowicki, S., Rahilly, K., Richardson, T., Rüdiger, J., Schipper, C.I., Watson, I.M., Wood, K., 2020. Aerial strategies advance volcanic gas measurements at inaccessible, strongly degassing volcanoes. Science. Advances 6, eabb9103.

Mandon, C.L., Christenson, B.W., Schipper, C.I., Seward, T.M., Garaebiti, E., 2019. Metal transport in volcanic plumes: a case study at White Island and Yasur volcanoes. J. Volcanol. Geotherm. Res. 369, 155–171.

Martin, R.S., Witt, M.L.I., Pyle, D.M., Mather, T.A., Watt, S.F.L., Bagnato, E., Calabrese, S., 2011. Rapid oxidation of mercury (Hg) at volcanic vents: insights from high temperature thermodynamic models of Mt Etna's emissions. Chem. Geol. 283, 279–286.

Mason, E., Wieser, P.E., Liu, E.J., Edmonds, M., Ilyinskaya, E., Whitty, R.C.W., Mather, T. A., Elias, T., Nadeau, P.A., Wilkes, T.C., McGonigle, A.J.S., Pering, T.D., Mims, F.M., Kern, C., Schneider, D.J., Oppenheimer, C., 2021. Volatile metal emissions from volcanic degassing and lava–seawater interactions at Kīlauea Volcano, Hawai'i. Communications Earth & Environment 2, 79.

Mather, T.A., Witt, M.L.I., Pyle, D.M., Quayle, B.M., Aiuppa, A., Bagnato, E., Martin, R.S., Sims, K.W.W., Edmonds, M., Sutton, A.J., Ilyinskaya, E., 2012. Halogens and trace metal emissions from the ongoing 2008 summit eruption of Kilauea volcano, Hawaii. Geochim. Cosmochim. Acta 83, 292–323.

McGonigle, A.J.S., Aiuppa, A., Giudice, G., Tamburello, G., Hodson, A.J., Gurrieri, S., 2008. Unmanned aerial vehicle measurements of volcanic carbon dioxide fluxes. Geophys. Res. Lett. 35, L06303.

Mori, T., Hashimoto, T., Terada, A., Yoshimoto, M., Kazahaya, R., Shinohara, H., Tanaka, R., 2016. Volcanic plume measurements using a UAV for the 2014 Mt. Ontake eruption. Earth Planets Space 68, 49.

Nriagu, J., 1989. A global assessment of natural sources of atmospheric trace metals. Nature 338, 47–49.

Poissant, L., Pilote, M., Beauvais, C., Constant, P., Zhang, H.H., 2005. A year of continuous measurements of three atmospheric mercury species (GEM, RGM and Hg_p) in southern Québec, Canada. Atmos. Environ. 39, 1275–1287.

Prestbo, E.M., Bloom, N.S., 1995. Mercury speciation adsorption (MESA) method for combustion flue gas: methodology, artifacts, intercomparison, and atmospheric implications. Water Air Soil Pollut. 80, 145–158.

Pyle, D.M., Mather, T.A., 2003. The importance of volcanic emissions for the global atmospheric mercury cycle. Atmos. Environ. 37, 5115–5124.

Rimondi, V., Chiarantini, L., Lattanzi, P., Benvenuti, M., Beutel, M., Colica, A., Costagliola, P., Di Benedetto, F., Gabbani, G., Gray, J.E., Pandeli, E., Pattelli, G., Paolieri, M., Ruggieri, G., 2015. Metallogeny, exploitation and environmental impact of the Mt. Amiata mercury ore district (Southern Tuscany, Italy). Ital. J. Geosci. 134, 323–336.

Rytuba, J.J., 2003. Mercury from mineral deposits and potential environmental impact. Environ. Geol. 43, 326–338.

Sæmundsson, K., Sigurgeirsson, M.A., Friðleifsson, G.O., 2020. Geology and structure of the Reykjanes volcanic system, Iceland. J. Volcanol. Geotherm. Res. 39, 106501.

Schiavo, B., Bermea-Morton, O., Salgado-Martinez, E., Arellano, J., Hernández-Álvarez, E., 2020. Estimates of mercury flux and temporal variability of Hg/SO_2 ratio in the plume of Popocatépetl volcano (Mexico). J. S. Am. Earth Sci. 101, 102614.

Schroeder, W.H., Munthe, J., 1998. Atmospheric mercury – an overview. Atmos. Environ. 32, 809–822.

Shinohara, H., Aiuppa, A., Giudice, G., Gurrieri, S., Liuzzo, M., 2008. Variation of H_2O/CO_2 and CO_2/SO_2 ratios of volcanic gases discharged by continuous degassing of Mount Etna volcano. Italy. Journal of Geophysical Research 113, B09203.

Sigurgeirsson, M.Á., Sæmundsson, K., 2022. Fagradalsfjall. In: Oladottir, B., Larsen, G., Guðmundsson, M.T. (Eds.), Catalogue of Icelandic Volcanoes. IMO, UI and CPD-NCIP. Retrieved from. https://icelandicvolcanoes.is/?volcano=FAG#.

Simmons, I.C., Pfeffer, M.A., Calder, E.S., Galle, B., Arellano, S., Coppola, D., Barsotti, S., 2017. Extended SO_2 outgassing from the 2014–2015 Holuhraun lava flow field, Iceland. Bull. Volcanol. 79, 79.

Sonke, J.E., Angot, H., Zhang, Y., Poulain, A., Björn, E., Schartup, A., 2023. Global change effects on biogeochemical mercury cycling. Ambio 52, 853–876.

Sprovieri, F., Pirrone, N., Bencardino, M., D'Amore, F., Carbone, F., Cinnirella, S., Mannarino, V., Landis, M., Ebinghaus, R., Weigelt, A., Brunke, E.G., Labuschagne, C., Martin, L., Munthe, J., Wangberg, I., Artaxo, P., Morais, F., Barbosa, H.D.J., Brito, J., Cairns, W., Barbante, C., Dieguez, M.D., Garcia, P.E., Dommergue, A., Angot, H., Magand, O., Skov, H., Horvat, M., Kotnik, J., Read, K.A., Neves, L.M., Gawlik, B.M., Sena, F., Mashyanov, N., Obolkin, V., Wip, D., Bin Feng, X., Zhang, H., Fu, X.W., Ramachandran, R., Cossa, D., Knoery, J., Marusczak, N., Nerentorp, M., Norstrom, C., 2016. Atmospheric mercury concentrations observed at ground-based monitoring sites globally distributed in the framework of the GMOS network. Atmos. Chem. Phys. 16, 11915–11935.

Stix, J., De Moor, J.M., Rüdiger, J., Alan, A., Corrales, E., D'Arcy, F., Diaz, J.A., Liotta, M., 2018. Using drones and miniaturized instrumentation to study degassing at Turrialba and Masaya Volcanoes, Central America. J. Geophys. Res. Solid Earth 123, 6501–6520.

Surl, L., Roberts, T., Bekki, S., 2021. Observation and modelling of ozone-destructive halogen chemistry in a passively degassing volcanic plume. Atmos. Chem. Phys. 21, 12413–12441.

Swartzendruber, P.C., Jaffe, D.A., Prestbo, E.M., Weiss-Penzias, P., Selin, N.E., Park, R., Jacob, D.J., Strode, S., Jaeglé, L., 2006. Observations of reactive gaseous mercury in the free troposphere at the Mount Bachelor Observatory. J. Geophys. Res. 111, D24302.

Tamburello, G., 2015. Ratiocalc: software for processing data from multicomponent volcanic gas analyzers. Comput. Geosci. 82, 63–67.

Thordarson, T., Höskuldsson, A., 2022. Classic Geology in Europe: Iceland, 3rd edition. London, Dunedin Academic Press.

Thordarson, T., Self, S., Miller, D.J., Larsen, G., Vilmundardóttir, E.G., 2003. Sulphur release from flood lava eruptions in the Veidivötn, Grímsvötn and Katla volcanic systems, Iceland. Geol. Soc. Lond. Spec. Publ. 213, 103–121.

US EPA, 1998. Method 7473—Mercury in Solids and Solutions by Thermal Decomposition, Amalgamation, and Atomic Absorption Spectrophotometry. Available online: https://www.epa.gov/sites/production/files/2015-07/documents/epa-7473.pdf (accessed 22 Dec 2021).

US EPA, 2016a. Method 30B—Mercury Sorbent Trap Procedure. Available online: https://www.epa.gov/sites/production/files/2017-08/documents/method_30b.pdf (accessed 12 Jan 2022).

US EPA, 2016b. Definition and Procedure for the Determination of the Method Detection Limit, Revision 2. Available online: https://www.epa.gov/sites/default/files/2016-12/documents/mdl-procedure_rev2_12-13-2016.pdf (accessed 23 Mar 2022).

Varekamp, J.C., Buseck, P.R., 1981. Mercury emissions from Mount St-Helens during September 1980. Nature 293, 555–556.

Varekamp, J.C., Buseck, P.R., 1986. Global mercury flux from volcanic and geothermal sources. Appl. Geochem. 1, 65–73.

Von Glasow, R., 2010. Atmospheric chemistry in volcanic plumes. Proceedings of the National Academy of Sciences USA 107, 6594–6599.

Wang, F., Outridge, P.M., Feng, X.B., Meng, B., Heimbürger-Boavida, L.E., Mason, R.P., 2019. How closely do mercury trends in fish and other aquatic wildlife track those in the atmosphere? – implications for evaluating the effectiveness of the Minamata Convention. Sci. Total Environ. 674, 58–70.

Wardell, L.J., Kyle, P.R., Counce, D., 2008. Volcanic emissions of metals and halogens from White Island (New Zealand) and Erebus volcano (Antarctica) determined with chemical traps. J. Volcanol. Geotherm. Res. 177, 734–742.

Werner, C., Christenson, B.W., Hagerty, M., Britten, K., 2006. Variability of volcanic gas emissions during a crater lake heating cycle at Ruapehu Volcano, New Zealand. J. Volcanol. Geotherm. Res. 154, 291–302.

Witt, M.L.I., Mather, T.A., Pyle, D.M., Aiuppa, A., Bagnato, E., Tsanev, V.I., 2008. Mercury and halogen emissions from Masaya and Telica volcanoes, Nicaragua. Journal of Geophysical Research–Solid Earth 113, B06203.

Zhang, Y., Zhang, P., Song, Z., Huang, S., Yuan, T., Wu, P., Shah, V., Liu, M., Chen, L., Wang, X., Zhou, J., Agnan, Y., 2023. An updated global mercury budget from a coupled atmosphere-land-ocean model: 40% more re-emissions buffer the effect of primary emission reductions. One Earth 6, 316–325.